Design Algorithms of Driving-Induced Nonreciprocal Components

Huanan Li and Tsampikos Kottos[*]

Wave Transport in Complex Systems Lab, Department of Physics, Wesleyan University, Middletown, Connecticut 06459, USA

We utilize an effective Hamiltonian formalism, within the Floquet scattering framework, to design a class of driving-induced nonreciprocal components with minimal complexity. In the high-driving-frequency limit, where our scheme is formally applicable, these designs demonstrate a leading-order nonreciprocal performance that is inversely proportional to the driving frequency. Surprisingly, the optimal nonreciprocal behavior persists also in the slow driving regime. Our approach highlights the importance of physical loops in the design of these driven nonreciprocal components.

I. INTRODUCTION

The quest for schemes that lead to the realization of novel nonreciprocal components has been, for many years now, a subject of intense activity [1–8]. On a fundamental level, these schemes must invoke mechanisms that violate time-reversal symmetry—the latter being in the core of wave transport reciprocity theorems [9–12]. On the technological level, the employed designs must satisfy a set of requirements; the nonreciprocal components must be bounded by the small footprint of the devices, be easily fabricated, have a small cost, have small energy consumption, etc. Needless to say that any achievement along these lines can influence the progress of wave transport management in areas as diverse as electromagnetism, acoustics, heat, matter, and quantum waves. At the same time, the development of a new class of circulators, isolators, and other nonreciprocal components will have dramatic implications in the next generation of communication, protection, imaging, and quantum information schemes.

In the electromagnetic framework, nonreciprocal transport has been mainly achieved via magneto-optical materials [13,14]. These exotic materials are normally very lossy when deposited on thin films. Moreover, the weak nature of the magneto-optical effects makes them incompatible with on-chip integration. Similar problems appear in acoustics, where magnetoacoustic effects are even weaker than their optical counterparts [15]. An alternative approach to directional wave transport utilizes nonlinear spatially asymmetric structures [1,6,16–22]. The nonlinear effects can be different for the forward- and backward-propagating waves, thus resulting in intensity-dependent propagation asymmetry. The same principle applies also for phononic heat transport and can lead to thermal diodes and rectifiers

[2,6,23,24]. Despite this success, nonlinear mechanisms impose limitations on the operational amplitude of the device—an undesirable feature from the engineering perspective. At the same time, in the case of electromagnetic and acoustic waves, they often introduce inherent signal distortions (generation of higher harmonics) [6].

Parallel approaches that aim to realize nonreciprocal components capitalize on active schemes. These designs utilize spatiotemporal modulations of the impedance profile of the propagating medium and provide a promising alternative for the realization of compact, reconfigurable nonreciprocal components [1,3,4,7,25–27]. In fact, when paired with the emerging field of Floquet engineering [28–30], they might provide a powerful approach that can produce frequency and bandwidth-tailored nonreciprocal transport [31,32].

In this paper, we utilize the toolbox of Floquet engineering, in order to design an efficient class of driving-induced nonreciprocal components with minimal complexity, i.e., nonreciprocal setups consisting of a minimal number of modes having the simplest connectivity; see Figs. 1(a) and 1(b). Our design scheme is demonstrated using the universal framework provided by coupled mode theory. Although it is formally applicable at the high-modulation-frequency limit, it also provides guidance for the design of nonreciprocal components in the low-frequency modulation regime. The proposed methodology highlights the importance of physical loops in these designs i.e., ring-like spatial configurations like the ones shown in Figs. 1(a) and 1(b) [33]. Moreover, it allows us to derive analytical expressions for the left and right transmittance asymmetry $\Delta = T_{L \to R} - T_{R \to L}$, which, in the high-frequency ω modulation regime, is $\Delta \sim \mathcal{O}(1/\omega)$. We find that the theoretical expressions that describe the transmittance asymmetry Δ of this class of isolators and circulators matches nicely with the numerical results and, in many occasions,
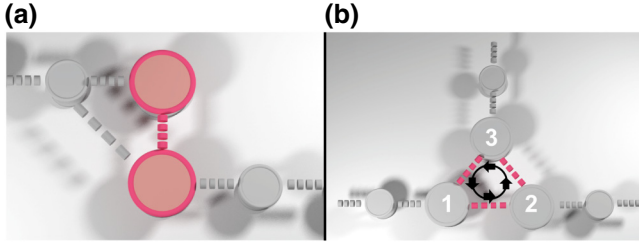
_____
[*]tkottos@wesleyan.edu

FIG. 1. Nonreciprocal components with $\mathcal{O}(1/\omega)$ performance consisting of a minimal number of modes having the simplest connectivity. Red highlights indicate the components which are potentially modulated in time. (a) An isolator based on two-mode modulated target. In the specific case, the modulated elements can be the resonant frequency of each mode and the coupling between them. (b) A circulator based on a three-mode target where the coupling between the modes is periodically modulated. The bold circle indicates the direction of circulation.

can reach the maximum value of 100% nonreciprocal behavior.

The structure of the paper is as follows. In Sec. II, we present the Floquet engineering scattering formalism in the limit of high modulation frequency. The method utilizes the notion of an effective Floquet Hamiltonian. In Sec. III, we implement this formalism for the design of reconfigurable nonreciprocal components with leading-order performance, which is inversely proportional to the driving frequency. In Sec. III A, we discuss the applicability of our scheme for the case of an isolator and demonstrate the validity of our approach via a specific model. The applicability of the method in the case of a circulator is shown in Sec. III B. In Sec. IV, we demonstrate the persistence of the optimal performance of our designs in the low-driving-frequency regimes via numerical examples. Finally, our conclusions are given in Sec. V.

II. FLOQUET SCATTERING IN THE HIGH-MODULATION-FREQUENCY LIMIT

We consider periodically time-modulated systems consisting of N_s coupled modes. In the context of coupled mode theory, such a (Hermitian) system can be described by a time-dependent N_s-dimensional Hamiltonian $\hat{H}_0(t) = \hat{H}_0^\dagger(t) = \hat{H}_0(t + T)$. It turns out that the evolution of such systems can be expressed in terms of an N_s-dimensional time-independent effective (Floquet) Hamiltonian $\hat{H}_F$ and a micromotion operator $\hat{U}_F(t) = \hat{U}_F(t + T)$ [28].

To clarify these notions of $\hat{H}_F$ and $\hat{U}_F$, we first introduce the one-period time-evolution operator $\hat{U}(t_0 + T, t_0)$ of the time-dependent Schrödinger-like equation $\iota \frac{d}{dt}|\psi(t)\rangle = \hat{H}_0(t)|\psi(t)\rangle$. This time-evolution operator $\hat{U}(t_0 + T, t_0)$ evolves states from an arbitrary initial time t_0 to time $t_0 + T$. The unitarity of $\hat{U}(t_0 + T, t_0)$ allows us to construct an orthonormal basis of the Hilbert space from its

eigenvectors. Specifically, we have

$$\hat{U}(t_0 + T, t_0)|\psi_\alpha(t_0)\rangle = e^{-\iota\varepsilon_\alpha T}|\psi_\alpha(t_0)\rangle, \qquad (1)$$

where $\{|\psi_\alpha(t_0)\rangle\}, \langle\psi_\beta(t_0)|\psi_\alpha(t_0)\rangle = \delta_{\beta\alpha}$ form a complete orthonormal basis and the real quasienergies ε_α are independent of the initial time t_0 and can be restricted to $\varepsilon_\alpha \in (-\omega/2, \omega/2]$ without loss of generality ($\omega \equiv 2\pi/T$). Starting from each specified initial state $|\psi_\alpha(t_0)\rangle$, we can evaluate the stationary solutions (Floquet states) $|\psi_\alpha(t)\rangle \equiv \hat{U}(t, t_0)|\psi_\alpha(t_0)\rangle$ of the aforementioned Schrödinger-like equation. These Floquet states can be written as

$$|\psi_\alpha(t)\rangle = |u_\alpha(t)\rangle e^{-\iota\varepsilon_\alpha t}, \qquad (2)$$

where $|u_\alpha(t)\rangle = |u_\alpha(t + T)\rangle$ are the so-called Floquet modes. Equation (2) constitutes the essence of the Floquet theorem.

Based on the quasienergies ε_α and the Floquet modes $|u_\alpha(t)\rangle$, we can define the one-point micromotion operator $\hat{U}_F(t)$ and the effective (Floquet) Hamiltonian $\hat{H}_F$ as [34]

$$\hat{U}_F(t) = \sum_\alpha |u_\alpha(t)\rangle\langle u_\alpha(0)|, \ \hat{H}_F = \sum_\alpha \varepsilon_\alpha|u_\alpha(0)\rangle\langle u_\alpha(0)|. \tag{3}$$

Notice that $\hat{U}_F(t) = \hat{U}_F(t + T)$ and, more importantly, the effective Hamiltonian $\hat{H}_F$ does not depend on the initial time t_0 since $|u_\alpha(0)\rangle = |\psi_\alpha(0)\rangle$ is an eigenvector of $\hat{U}(T, 0)$. Finally, using Eq. (3), we can express the general time-evolution operator $\hat{U}(t, t_0) = \sum_\alpha |\psi_\alpha(t)\rangle\langle\psi_\alpha(t_0)|$ in the form

$$\hat{U}(t, t_0) = \hat{U}_F(t) e^{-\iota\hat{H}_F(t-t_0)} \hat{U}_F^\dagger(t_0), \qquad (4)$$

where the dependence on t_0 is attributed to the one-point micromotion operator. From the above discussion, it becomes clear that $\hat{H}_F$ describes the long time (stroboscopic) dynamics, while $\hat{U}_F$ accounts for the evolution within one period of the driving.

The effective Hamiltonian formalism allows us to invoke a systematic high-frequency expansion in ω for both the effective Hamiltonian $\hat{H}_F$ and the micromotion operator $\hat{U}_F(t)$ [29]. A benefit of this representation is the fact that one can eliminate the artificial dependence of the effective Hamiltonian on the driving phase (i.e., the initial time of periodic driving), which can be elusive as far as symmetry preservation is concerned [29].

At the same time, the notion of $\hat{H}_F$ and $\hat{U}_F$ has been proven useful in the analysis of Floquet scattering settings [32]. The latter constitutes the natural framework where the scattering properties of driven targets can be inferred from the dynamics of their isolated (i.e., in the absence of coupling with leads) counterparts [31]. The

proposed approach [32] allows us to treat the driven target as a static one—which is described by the effective Hamiltonian $\hat{H}_F$—coupled to leads. In this framework, the coupling constants that describe the coupling of the target with the leads are also time independent—albeit they are different from their bare values due to a renormalization procedure that involves information encoded in the micromotion.

To be specific, we consider a time-periodic driven target that is coupled with M identical leads. The coupling strengths between the target and the leads are given by the bare coupling matrix $\hat{c}$. The transport characteristics of this system are given by the Floquet scattering matrix $\mathcal{S}$, which couples the outgoing propagating channels with the incoming ones. Below, we assume for simplicity that in the high-driving-frequency domain there exists only one propagating channel in each lead. The case of multimode leads, although more cumbersome, can also be worked out along the same lines. The flux-normalized scattering matrix S, up to order $\mathcal{O}\left(1/\omega^2\right)$, is [32]

$$S \approx -I_M + \iota v_g \hat{c}_u G \hat{c}_u^{\dagger}, \quad G = \frac{1}{E - \hat{H}_F + \Lambda_u + \frac{\iota}{2} v_g \hat{c}_u^{\dagger} \hat{c}_u}, \tag{5}$$

where I_M is the $M \times M$ identity matrix, $v_g = \partial E / \partial k$ is the group velocity of the propagating channel, and $\hat{c}_u = \hat{c}\hat{u}_0$ is the renormalized bare coupling due to the micromotion $\hat{u}_n \equiv (1/T) \int_0^T dt \hat{U}_F(t) e^{\iota n \omega t}$. The latter can be approximated as

$$\hat{u}_n \approx \begin{cases} I_{N_s} - \frac{1}{2\omega^2} \sum_{m \neq 0} \frac{1}{m^2} \hat{H}^{(-m)} \hat{H}^{(m)}; & n = 0, \\ \frac{1}{n\omega} \hat{H}^{(n)}; & n \neq 0, \end{cases} \tag{6}$$

where $\hat{H}^{(n)} \equiv (1/T) \int_0^T dt \hat{H}_0(t) e^{\iota n \omega t}$. The term $\Lambda_u = \lambda \hat{c}_u^{\dagger} \hat{c}_u + \sum_n \hat{u}_n^{\dagger} \iota \hat{\Gamma} \hat{u}_n$ in the denominator of Eq. (5) represents the fact that the target is not isolated. The origin of these two terms is different: the first one describes the channel-coupling-induced renormalization to the closed-system Hamiltonian while the second one is optional and describes potential material gain and/or loss of the target ($-\iota \hat{\Gamma}$ is a non-Hermitian diagonal matrix). In fact, in an alternative formulation of the problem, we could absorb the gain and/or loss properties of the isolated system in a composite coupled mode Hamiltonian $\hat{H}_0(t) \rightarrow \hat{H}_0(t) - \iota \hat{\Gamma}$ with a corresponding $\hat{H}_F \rightarrow \hat{H}_F - \iota \sum_n \hat{u}_n^{\dagger} \hat{\Gamma} \hat{u}_n$.

Finally, the high-frequency expansion of the effective Hamiltonian $\hat{H}_F$ is given in many references [32,35], and it is shown here for the sake of completeness and convention

consistency:

$$\begin{aligned} \hat{H}_F \approx \hat{H}^{(0)} &- \sum_{n=1}^{\infty} \frac{1}{n\omega} \left[\hat{H}^{(n)}, \hat{H}^{(-n)} \right] \\ &+ \sum_{n \neq 0} \frac{\left[\hat{H}^{(-n)}, \left[\hat{H}^{(0)}, \hat{H}^{(n)} \right] \right]}{2n^2 \omega^2} \\ &+ \sum_{n \neq 0} \sum_{n' \neq 0, n} \frac{\left[\hat{H}^{(-n')}, \left[\hat{H}^{(n'-n)}, \hat{H}^{(n)} \right] \right]}{3nn' \omega^2}. \end{aligned} \tag{7}$$

Hereafter, we consider tight-binding leads with dispersion relation $E(k) = -2\cos(k)$ (in units of coupling). In this case, $\lambda = \cos(k)$ (appearing in Λ_u) and the group velocity $v_g = 2\sin(k)$, where $k \in (0, \pi)$.

Finally, we point out the structural similarities between the S-matrix given by Eq. (5) and the scattering matrix associated with static targets, when the latter is written in terms of the Hamiltonian of the corresponding isolated system; see, for example, Refs. [36] and [37]. These similarities can be proven useful in other investigations where scattering properties of complex and/or chaotic systems are investigated. Interestingly enough, although the formula Eq. (5) is formally correct up to order $\mathcal{O}\left(1/\omega^2\right)$, its performance typically goes beyond this order [compare, for example, Figs. 2(b) and 2(a)]. The reason is subtle, but we might appreciate it from the preserved structure and general properties. For example, in the absence of gain and loss, i.e., $\hat{\Gamma} = 0$, the approximate scattering matrix in Eq. (5) preserves the unitarity as it should.

Below, we present our design strategy for the realization of nonreciprocal components with $\mathcal{O}(1/\omega)$ performance [see Figs. 1(a) and 1(b)]. It consists of two steps: first, we utilize the Floquet engineering within the scattering setup to develop driving schemes that provide optimal nonreciprocal responses in the high-frequency limit. In the second step, we demonstrate that these same designs manifest optimal transmittance asymmetry also in the limit of slow driving. Our proposal is supported by detailed simulations.

III. NONRECIPROCAL COMPONENTS IN THE HIGH-FREQUENCY LIMIT

First, we utilize Eq. (5) to derive analytical expressions for the left and right transmittance asymmetry Δ up to leading order in driving frequency ω, i.e., $\Delta \propto \mathcal{O}(1/\omega)$. A subsequent optimization of these expressions with respect to various driving parameters allows us to engineer nonreciprocal components (circulators, isolators) with maximum transmittance asymmetry.
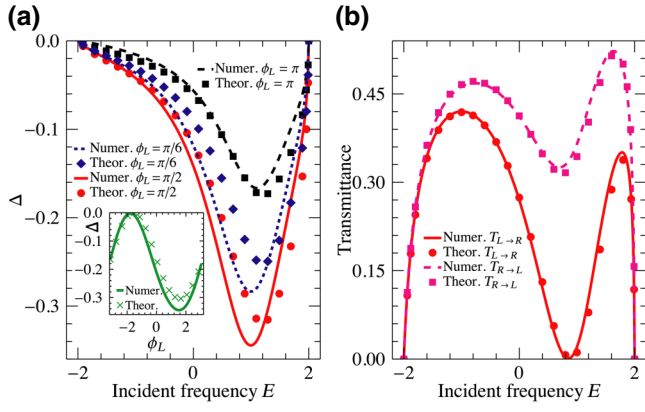
FIG. 2. Nonreciprocal characteristics of a two-mode driven isolator with a physical loop [see Fig. 1(a)]. The driving protocol is given by Eq. (9). (a) The numerical (lines) values (using the Floquet scattering matrix approach; see Ref. [31]), for the transmittance asymmetry Δ versus the incident frequency E, are compared with the theoretical (symbols) results of Eq. (8). Three different relative driving phases for the left resonator $\phi_L = \pi$, $\pi/2$, and $\pi/6$ are studied. The best isolation performance is observed when $\phi_L = \pi/2$ (see also the inset). Inset: The transmittance asymmetry Δ versus the phase ϕ_L when the incident frequency is fixed to be $E = 1$. (b) Left/right transmittances $(T_{L \rightarrow R}/T_{R \rightarrow L})$ versus the incident frequency E when the optimized phase $\phi_L = \pi/2$ is used. The theoretical result (symbols) are given by Eq. (5). In both (a) and (b), we use the following set of parameters associated with the driving protocol Eq. (9): $\varepsilon_L^0 = \varepsilon_R^0 = 0, f_L = f_R = 1, \phi_R = -\pi/2, h_0 = -2h = -1, \omega = 6$, and finally $\gamma = 0.3$ for the uniform loss. The bare coupling matrix that describes the coupling between the target and the leads has matrix elements $c_L = c_R = \tilde{c}_L = -1$.

A. Reconfigurable isolators

The first reconfigurable nonreciprocal component that we design is an isolator. We consider the simplest possible scenario involving two driving modes, i.e., $N_s = 2$, coupled to two leads $M = 2$ [38]. We first observe that the leading-order contribution $\propto \mathcal{O}(1/\omega)$ in the expression Eq. (5) for the scattering matrix originates solely from the effective Floquet Hamiltonian $\hat{H}_F$ [see Eq. (7)]. Because of its Hermitian nature, however, the 2×2 matrix $\hat{H}_F$ cannot lead to a transmittance asymmetry $|S_{12}| \neq |S_{21}|$. One needs, therefore, to "break" this Hermiticity constraint—an operation performed by incorporating in $\hat{H}_F$ the non-Hermitian diagonal matrix $\imath \hat{\Gamma}$ (see previous discussion). As a result, the matrix G in Eq. (5) has, up to a common factor, complex diagonal matrix elements $G_{11}, G_{22} \in \mathcal{C}$, while its off-diagonal elements are complex conjugates of each other: $G_{12} = G_{21}^*$. This, by itself, does not guarantee that $|S_{21}| \neq |S_{12}|$, let alone that $\Delta \propto \mathcal{O}(1/\omega)$. The latter requirement can be fulfilled only when the bare coupling matrix $\hat{c}$ has off-diagonal elements that lead to a mixing of diagonal and off-diagonal terms of G after performing the multiplication [see Eq. (5)]. The

presence of off-diagonal elements in $\hat{c}$ suggests an isolator design that involves physical loops. An example of such a system is shown in Fig. 1(a) and it is mathematically modeled via the bare coupling matrix $\hat{c} = \left(\begin{smallmatrix} c_L & \tilde{c}_L \\ 0 & c_R \end{smallmatrix}\right)$. We stress again that this design is a direct consequence of the theoretical analysis of Eq. (5).

Next, we proceed with the evaluation of transmittance asymmetry Δ for the design of Fig. 1(a). For simplicity, we assume uniform gain or loss, i.e., $\hat{\Gamma} = \gamma I_{N_s}$. Furthermore, we parametrize the effective Hamiltonian $\hat{H}_F$ as $\hat{H}_F = \hat{H}_F^\dagger = \left(\begin{smallmatrix} \eta_1 & \eta_r + \imath \eta_i \\ \eta_r - \imath \eta_i & \eta_2 \end{smallmatrix}\right)$ and the micromotion operator $\hat{u}_0$ as $\hat{u}_0 = \hat{u}_0^\dagger = \left(\begin{smallmatrix} \mu_1 & \mu_r + \imath \mu_i \\ \mu_r - \imath \mu_i & \mu_2 \end{smallmatrix}\right)$. In the above parametrization, we consider terms up to order $\mathcal{O}(1/\omega^2)$. Specifically, since the target in the absence of modulation is reciprocal, we have that $\eta_i \sim \mathcal{O}(1/\omega)$, while generally $\{\eta_1, \eta_2, \eta_r\} \sim \mathcal{O}(1)$. Similarly, the components of the micromotion operator $\hat{u}_0$ are $\mu_{1,2} = 1 + \mathcal{O}(1/\omega^2)$ and $\mu_{r,i} \sim \mathcal{O}(1/\omega^2)$.

It turns out that the matrix elements η_i and μ_i are essential for the presence of the transmittance asymmetry. Their origins are traced back to the presence of driving and can be associated with an effective gauge field [40]. To appreciate the importance of η_i and μ_i, we evaluate the transmittance asymmetry Δ explicitly up to $\mathcal{O}(1/\omega^2)$. Using Eq. (5), we get

$$\Delta \approx -\frac{4c_L c_R^2 v_g^2 \gamma \left\{ \eta_i \tilde{c}_L + \mu_i \left[\tilde{c}_L (\eta_1 - \eta_2) - 2c_L \eta_r \right] \right\}}{|\det D(\gamma)|^2}$$
$$\propto \eta_i + \mathcal{O}(1/\omega^2), \tag{8}$$

where the matrix $D(\gamma) \equiv E + \imath \gamma - \hat{H}_F + e^{\imath k} \hat{c}^\dagger \hat{c}$ and $\hat{H}_F$ is evaluated using the first two terms in Eq. (7).

Let us now consider a specific driving protocol described by the time-dependent Hamiltonian $\hat{H}_0(t)$:

$$\hat{H}_0(t) = \begin{pmatrix} \varepsilon_L(t) & h(t) \\ h(t) & \varepsilon_R(t) \end{pmatrix}, \tag{9}$$

where $\varepsilon_{L/R}(t) = \varepsilon_{L/R}^0 + 2f_{L/R}\cos(\omega t + \phi_{L/R})$ and $h(t) = h_0 + 2h\cos(\omega t + \phi_0)$. For the specific driving protocol of Eq. (9), we have that $\mu_i \sim \mathcal{O}(1/\omega^3)$, $\eta_i = (2h/\omega)[f_L \sin(\phi_L - \phi_0) - f_R \sin(\phi_R - \phi_0)] + \mathcal{O}(1/\omega^3)$, and $\hat{H}_F = \left(\begin{smallmatrix} \varepsilon_L^0 & h_0 + \imath \eta_i \\ h_0 - \imath \eta_i & \varepsilon_R^0 \end{smallmatrix}\right) + \mathcal{O}(1/\omega^2)$. Without any loss of generality, we assume that the starting time of the driving scheme is such that $\phi_0 = 0$. Then the other two driving phases $\phi_{L/R}$ can be measured *relative* to ϕ_0 and used to optimize the transmittance asymmetry. A theoretical expression for the transmittance asymmetry Δ, as a function of incident frequency E, can be calculated by direct substitution of μ_i, η_i into Eq. (8). Specifically we find that in the leading order $\mathcal{O}(1/\omega)$, the following expression for the transmittance

asymmetry

$$\Delta \approx -\frac{8c_L c_R^2 \tilde{c}_L v_g^2 \gamma h}{\left|\det D(\gamma)|_{\omega\to\infty}\right|^2} \frac{(f_L \sin\phi_L - f_R \sin\phi_R)}{\omega}, \quad (10)$$

which takes its maximum value $|\Delta|$ for $\phi_L = -\phi_R = \pi/2$.

In Fig. 2(a), we report the theoretical predictions Eq. (8) for the transmittance asymmetry Δ, together with the outcome of the simulations (where the exact Floquet scattering matrix is used [31]). Various values of the driving phases $\phi_L = \pi, \pi/2, \pi/6$ (for fixed $\phi_R = -\pi/2$) are considered. In all cases, we observe a nice agreement between theory and numerics. Moreover, we find that the maximal transmittance asymmetry occurs when $\phi_L \approx \pi/2$, as predicted by our theory. This optimal phase choice is further verified in the inset of Fig. 1(a), where we report Δ versus ϕ_L for a fixed-incident wave frequency $E = 1$. In Fig. 2(b), we also report the individual left $T_{L\to R}$ and right $T_{R\to L}$ transmittances versus the incident wave frequency, for the optimized phase configuration $\phi_L = -\phi_R = \pi/2$. The theoretical results (symbols) are calculated using the (approximated) expression Eq. (5) for the S-matrix (high-frequency limit).

At this point, we would like to bring attention to the fact that the correspondence between theory and numerics in Fig. 2(b) is superior to the one found in Fig. 2(a). To this end, we recall that both theoretical results associated with Eq. (5) and the first equality in Eq. (8) are formally correct up to order $\mathcal{O}(1/\omega^2)$. Nevertheless, they also incorporate higher-order terms in $1/\omega$. It turns out that some of these terms, which are present in Eq. (5) and excluded when evaluating Eq. (8), are responsible for this deterioration of the agreement between theory and numerics in Fig. 2(a). We speculate that the unitarity relation that holds in Eq. (5) (in the absence of loss) imposes some additional constraints on the higher orders that are responsible for the better agreement with the numerics. In a sense, the structure of Eq. (5) reminds us of a Padé approximation for the scattering matrix in a $1/\omega$ asymptotic series. It will indeed be very interesting to pursue such a possibility further. This pursuit, however, is beyond the scope of the current paper.

Let us finally discuss in more detail the accuracy of the theoretical results of Eq. (10) for the transmittance asymmetry Δ. Indeed, we find that, for this specific model, the $\det D(\gamma)$ that appears in Eq. (8) can be expanded as $\det D(\gamma) = \det D(\gamma)|_{\omega\to\infty} + \mathcal{O}(1/\omega^2)$. As a result, we conclude that the accuracy of the theoretical result Eq. (10) is up to the order $\mathcal{O}(1/\omega^2)$. We confirm this prediction using detailed numerical simulations; see Fig. 3. In the inset of the same figure, we report the error between Eq. (10) and the exact numerical data evaluated from the Floquet scattering matrix, which shows an $\mathcal{O}(1/\omega^3)$ scaling, in agreement with our prediction.
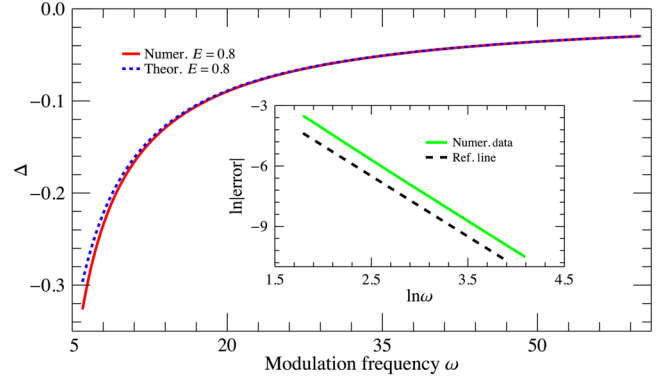

FIG. 3.   (a) The transmittance asymmetry Δ versus the modulation frequency ω for the specific example of Eq. (9). The theoretical results of Eq. (10) are compared with the results of the simulations from the (exact) Floquet scattering matrix. The difference between theoretical and numerical results for Δ (indicated as |error| in the inset), turns out to be $\mathcal{O}(1/\omega^3)$; see the black dashed reference line in the inset, which has slope -3. The other parameters are the same as in Fig. 2(b).

B. Reconfigurable circulators

We proceed with the design of circulators. As before, we consider a design with the minimal complexity consisting of three (driven) modes, each of which is coupled to a lead (i.e., $M = 3$) with equal coupling strength c. As opposed to the case of (two-channel) isolators, here the presence of the non-Hermitian term $\hat{\Gamma}$ (describing material gain and/or loss) is not necessary. The non-Hermiticity is automatically satisfied by the presence of the propagating channel in the third lead and, thus, we will assume below that $\hat{\Gamma} = 0$. In the absence of driving, the system is respecting a rotational symmetry. We want to design a counterclockwise circulator, i.e., a three-port structure for which counterclockwise transmittances $T_{21}, T_{32}, T_{13} \neq 0$, while transmittances in the clockwise direction are (essentially) zero, i.e., $T_{31}, T_{23}, T_{12} \approx 0$. Obviously, such a structure must demonstrate a strong *positive* transmittance asymmetry $\Delta > 0$ between two consequent leads. A schematics of this circulator is shown in Fig. 1(b).

Similar to the case of the isolator, we parametrize the effective Hamiltonian $\hat{H}_F$ as

$$\hat{H}_F = \begin{pmatrix} \eta_{01} & \eta_{1r} + \iota\eta_{1i} & \eta_{3r} - \iota\eta_{3i} \\ \eta_{1r} - \iota\eta_{1i} & \eta_{02} & \eta_{2r} + \iota\eta_{2i} \\ \eta_{3r} + \iota\eta_{3i} & \eta_{2r} - \iota\eta_{2i} & \eta_{03} \end{pmatrix}, \quad (11)$$

where $\eta_{ni} \sim \mathcal{O}(1/\omega)$; $\eta_{0,n} = \epsilon_0 + \mathcal{O}(1/\omega)$; $\eta_{n,r} = h_0 + \mathcal{O}(1/\omega)$; and $n = 1, 2, 3$. At the same time the micromotion operator $\hat{u}_0$ can be written as

$$\hat{u}_0 = \begin{pmatrix} \mu_{01} & \mu_{1r} + \iota\mu_{1i} & \mu_{3r} - \iota\mu_{3i} \\ \mu_{1r} - \iota\mu_{1i} & \mu_{02} & \mu_{2r} + \iota\mu_{2i} \\ \mu_{3r} + \iota\mu_{3i} & \mu_{2r} - \iota\mu_{2i} & \mu_{03} \end{pmatrix}, \quad (12)$$

with $\mu_{0n} = 1 + \mathcal{O}\left(1/\omega^2\right)$; $\{\mu_{nr}, \mu_{ni}\} \sim \mathcal{O}\left(1/\omega^2\right)$; and $n = 1, 2, 3$.

From Eqs. (5), (11), and (12), we are able to derive the following expression for the transmittance asymmetry Δ up to $\mathcal{O}\left(1/\omega^2\right)$ between two consequent leads [say, lead 1 and lead 2; see Fig. 1(b)]:

$$\Delta \approx \frac{\left(c^2 v_g\right)^3 \left(h_\eta + m_\mu\right)}{|\det D\left(0\right)|^2} \propto h_\eta + \mathcal{O}(1/\omega^2), \qquad (13)$$

where the matrix $D(\gamma)$ is defined below Eq. (8). Above, $h_\eta \equiv 2\left(\eta_{1r}\eta_{2r}\eta_{3i} + \eta_{3r}\eta_{1r}\eta_{2i} + \eta_{2r}\eta_{3r}\eta_{1i}\right)$ originates from the effective Hamiltonian $\hat{H}_F$ and $m_\mu \equiv 4h_0^2\left(h_0 - \varepsilon_0 - 2\cos k\right)\sum_n \mu_{ni}$ from the micromotion. Because of the structural symmetry of the undriven system, Eq. (13) applies also for the transmittance asymmetry between the leads 2 (3) and 3 (1).

Let us work out a specific driving protocol described by the following time-periodic Hamiltonian:

$$\hat{H}_0\left(t\right) = \begin{pmatrix} \varepsilon_0 & h_1\left(t\right) & h_3\left(t\right) \\ h_1\left(t\right) & \varepsilon_0 & h_2\left(t\right) \\ h_3\left(t\right) & h_2\left(t\right) & \varepsilon_0 \end{pmatrix}, \qquad (14)$$

where the periodic modulation pertains to the couplings $h_n\left(t\right) = h_0 + 2h\cos\left(\omega t + \phi_n\right)$. We want to identify the driving phases' configuration $\{\phi_n\}$ for which the circulator will demonstrate maximum performance. In this case, we have that $\mu_{ni} \sim \mathcal{O}\left(1/\omega^3\right)$, $\eta_{nr} = h_0 + \mathcal{O}\left(1/\omega^2\right)$, $\eta_{1i} = (2h^2/\omega)\sin\left(\phi_3 - \phi_2\right) + \mathcal{O}\left(1/\omega^3\right)$ [and cyclically $\eta_{2i} = (2h^2/\omega)\sin\left(\phi_1 - \phi_3\right) + \mathcal{O}\left(1/\omega^3\right)$, etc.] [41]. According to Eq. (13), the associated transmittance asymmetry reads

$$\Delta \approx \frac{4h_0^2 h^2 \left(c^2 v_g\right)^3 \left(\sin\left(\phi_2 - \phi_1\right) + \sin\left(\phi_1 - \phi_3\right) + \sin\left(\phi_3 - \phi_2\right)\right)}{\omega |\det D\left(0\right)|^2}. \qquad (15)$$

The above equation indicates that Δ depends only on the relative driving phases, i.e., $\phi_2 - \phi_1$ and $\phi_3 - \phi_1$. Without loss of generality, we set $\phi_1 = 0$. From Eq. (15), we find that the phase configuration $\phi_2 = 2\pi/3$ and $\phi_3 = 4\pi/3$ (or similarly $\phi_2 = 4\pi/3$ and $\phi_3 = 2\pi/3$) can produce the maximum asymmetry up to order $\mathcal{O}\left(1/\omega\right)$. We point out that a similar driving phase configuration has been implemented recently in the case of mode-modulated circulators [42]—though, in our case, it is important to realize that this optimal configuration emerged as a result of our optimization approach. We can further optimize Δ with respect to the coupling parameter c. It turns out that, for the specific case of optimal phases, the critical coupling (perfect impedance matching) occurs for $c \approx -0.5$.

In Fig. 4(a), we show the numerical data for the transmission asymmetry Δ between channels 1 and 2 [see Fig. 1(b)] versus the incident frequency for the optimal
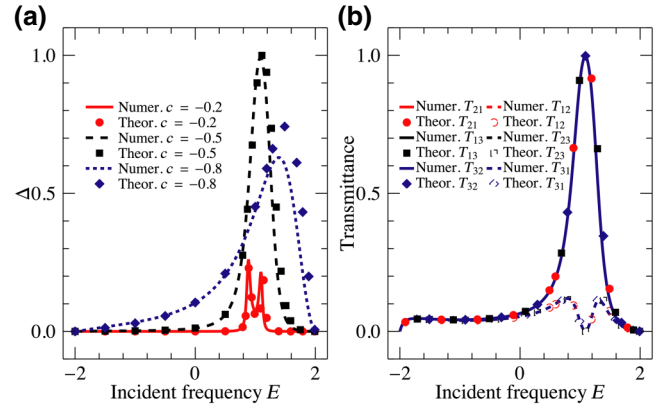

FIG. 4. (a) Nonreciprocal transmittance Δ between leads 1 and 2 [see Fig. 1(b)] for the model Eq. (14). An optimal phase configuration $\phi_1 = 0$, $\phi_2 = 2\pi/3$, and $\phi_3 = 4\pi/3$ and various coupling constants c are considered. Maximum nonreciprocity $\Delta = 1$ is achieved for perfect impedance, matching conditions corresponding to $c \approx -0.5$ (and $E \approx 1.1$). The numerical data (lines) are derived using the (exact) Floquet scattering matrix; see Ref. [31]. The theoretical results (symbols) correspond to Eq. (15). (b) The transmittances $T_{nn'} = |S_{nn'}|^2$ in a clockwise or counterclockwise direction versus the incident frequency E when the coupling $c = -0.5$. The theoretical results (symbols) Eq. (5) match perfectly the numerical results (lines). The other parameters for both (a) and (b) are $h_0 = -1, h = 0.5, \varepsilon_0 = 0$, and $\omega = 6$.

phase configuration $\phi_1 = 0$, $\phi_2 = 2\pi/3$, and $\phi_3 = 4\pi/3$. Various coupling strengths c are considered. In the same figure, we also report the theoretical results for Δ; see Eq. (15). We find a nonmonotonic behavior of the transmittance asymmetry with respect to the coupling c due to the impedance mismatch. For the predicted coupling $c \approx -0.5$, the system demonstrates a nonreciprocal behavior, which is as high as 100%.

The individual transmittances $T_{nn'} = |S_{nn'}|^2$ versus incident frequency E (for the optimal phase and coupling configurations) are reported in Fig. 4(b). Both theoretical [using Eq. (5)] and numerical (using the exact Floquet scattering matrix [31]) results fall nicely one on top of the other and indicate that, for the optimal phase configuration, $T_{31} = T_{23} = T_{12} \approx 0$, while $T_{21} = T_{32} = T_{13} \neq 0$ at a frequency range around $E \approx 1.1$.

Similar to the case of isolators, we evaluate the accuracy of the theoretical results of Eq. (15) for the transmittance asymmetry Δ versus the modulation frequency ω; see Fig. 5. In the same figure, we report the numerical results (using the Floquet scattering matrix) for Δ. Since our theoretical expression Eq. (15) is accurate up to the order $\mathcal{O}\left(1/\omega^2\right)$, we expect that the error, i.e., the deviation between the theoretical and the exact numerical result for Δ, has to scale as $\mathcal{O}\left(1/\omega^3\right)$. These expectations are nicely confirmed by our detail numerical analysis; see the inset of Fig. 5.
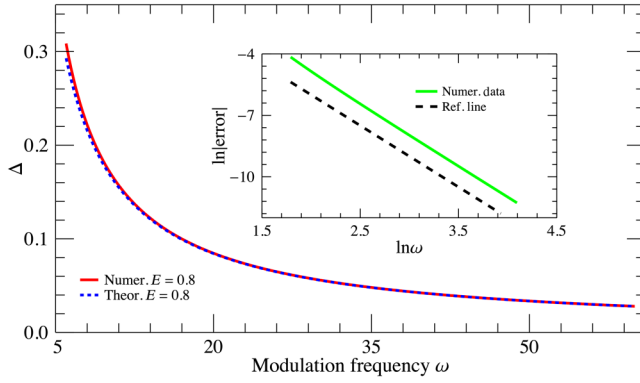
FIG. 5. The transmittance asymmetry Δ versus the modulation frequency ω for the specific example Eq. (14) of the circulator. The theoretical results of Eq. (15) are compared with the results of the simulations from the (exact) Floquet scattering matrix. The difference between theoretical and numerical results for Δ (indicated as |error| in the inset) is $\mathcal{O}\left(1/\omega^3\right)$; see the black dashed reference line in the inset, which has slope -3. The other parameters are the same as in Fig. 4(b).

IV. NONRECIPROCAL COMPONENTS IN THE LOW-DRIVING-FREQUENCY LIMIT

Although the Floquet S-matrix can be always expressed in terms of $\hat{H}_F$, one can no longer use the approximated forms Eqs. (5)–(7) in the slow-frequency-driving limit. As a result, our theoretical expressions Eqs. (8) and (13) for the transmittance asymmetry are no longer
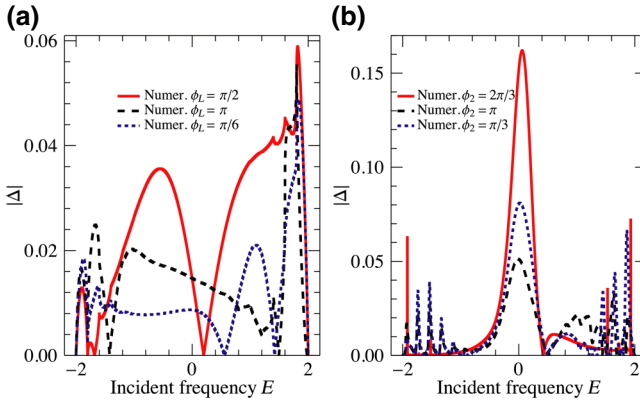

FIG. 6. Performance of nonreciprocal components in the low-driving-frequency limit $\omega = 0.2$. (a) Isolator: The magnitude of the transmittance asymmetry $|\Delta|$ versus the incident frequency E when $\phi_L = \pi, \pi/2$, and $\pi/6$, respectively. The model for the isolator and the other parameters are the same as in Fig. 2. (b) Circulator: The magnitude of the transmittance asymmetry $|\Delta|$ versus the incident frequency E when $\phi_2 = 2\pi/3, \pi$, and $\pi/3$, while $\phi_1 = 0$ and $\phi_3 = 4\pi/3$ are kept fixed. The design of the circulator and the other parameters are the same as in Fig. 4(b). As shown in panels (a) and (b), the relative driving phases for the (overall) optimal performance of the nonreciprocal components are consistent with the high-driving-frequency prediction.

applicable. We find, nevertheless, that the driving designs that lead to optimal nonreciprocity in the case of high-frequency-driving schemes are applicable even in the case of small driving frequencies. This conclusion is supported via detailed numerical simulations for various drivings. Typical examples are shown in Figs. 6(a) and 6(b), where we plot the numerical results for $|\Delta|$ (using the exact Floquet scattering matrix [31]) for the previous designs of isolators and circulators. A small driving frequency $\omega = 0.2$ is now used. In the case of an isolator [see Fig. 6(a)], we report $|\Delta(E)|$ for three representative driving phases $\phi_L = \pi, \pi/2, \pi/6$. An overall optimal asymmetric transmittance is observed for $\phi_L = \pi/2$, which is the predicted optimal phase in the case of high-frequency-driving schemes (see Fig. 2). Similarly, in Fig. 6(b), we report the behavior of $|\Delta(E)|$ for $\phi_1 = 0$; $\phi_3 = 4\pi/3$; and various values of $\phi_2 = 2\pi/3$, π, and $\pi/3$. Again, we find that an overall optimal transmittance asymmetry is observed when $\phi_2 = 2\pi/3$, which is the predicted optimal driving phase in the case of high-frequency-driving schemes.

V. CONCLUSION

We develop a scheme for designing optimal nonreciprocal components (isolators, circulators, etc.) that utilizes the concept of Floquet engineering. In the high-modulation-frequency limit, we develop a theoretical formalism that relies on the notion of effective Floquet Hamiltonians $\hat{H}_F$ and allows us to express the transmittance asymmetry in inverse powers of the modulation frequency. An analysis of the theoretical expressions provides guidance for the geometrical design of nonreciprocal components and driving schemes that can lead to optimal performance. Specifically, the method highlights the importance of physical loops in getting maximum nonreciprocal efficiency. A detailed numerical investigation indicates that these designs can provide optimal nonreciprocal transport even in the case of low driving frequencies.

Our approach can find promising applications in the framework of classical electromagnetic and acoustic wave physics. In the microwave (or rf) regime, for example, one can implement the time-modulated coupling between LC resonators (or the resonance frequency modulations of the LC resonators) via capacitance modulation achieved with varactor diodes [42,43]. In the acoustic framework, one can use actuators that compress elastically the acoustic medium filling the coupled cavities (or the coupling channels between these cavities) in order to impose a temporal modulation of their effective acoustic index by weak variations of their volumes [44]. Other potential applications could be in the framework of matter wave physics as well as thermal transport, where the design of reconfigurable thermal diodes is a challenging research direction.

----

[1] R. Fleury, D. Sounas, M. R. Haberman, and A. Alú, Nonreciprocal acoustics, Acoust. Today **11**, 14 (2015).

[2] N. Li, J. Ren, L. Wang, G. Zhang, P. Hänggi, and B. Li, Phononics: Manipulating heat flow with electronic analogs and beyond, Rev. Mod. Phys. **84**, 1045 (2012).

[3] C. Caloz, A. Alú, S. Tretyakov, D. Sounas, K. Achouri, and Z.-L. Deck-Léger, Electromagnetic Nonreciprocity, Phys. Rev. Appl. **10**, 047001 (2018).

[4] D. L. Sounas and A. Alú, Non-reciprocal photonics based on time modulation, Nat. Photonics **11**, 774 (2017).

[5] A. B. Khanikaev and A. Alú, Optical isolators: Nonlinear dynamic reciprocity, Nat. Phot. **9**, 359 (2015).

[6] A. A. Maznev, A. G. Every, and O. B. Wright, Reciprocity in reflection and transmission: What is a 'phonon diode'? Wave Motion **50**, 776 (2013).

[7] Z. Yu and S. Fan, Optical Isolation: A non-magnetic approach, Nat. Photonics **5**, 517 (2011).

[8] Y. Shi, Z. Yu, and S. Fan, Limitations of nonlinear optical isolators due to dynamic reciprocity, Nat. Phot. **9**, 388 (2015).

[9] L. D. Landau and E. M. Lifshitz, *Electrodynamics of Continuous Media* (Addison-Wesley, Reading, MA, 1960).

[10] H. B. G. Casimir, On Onsager's principle of microscopic reversibility, Rev. Mod. Phys. **17**, 343 (1945).

[11] H. A. Haus, *Waves and Fields in Optoelectronics* (Prentice-Hall, Englewood Cliffs, NJ, 1984).

[12] B. E. A. Saleh and M. C. Teich, *Fundamentals of Photonics* (Wiley InterScience, Hoboken, NJ, 2007).

[13] A. K. Zvezdin and V. A. Kotov, *Modern Magneto-optics and Magneto-optical Materials* (Taylor & Francis, London, 1997).

[14] H. Dötsch, N. Bahlmann, O. Zhuromskyy, M. Hammer, L. Wilkens, R. Gerhardt, P. Hertel, and A. F. Popkov, Applications of magneto-optical waveguides in integrated optics: Review, J. Opt. Soc. Am. B **22**, 240 (2005).

[15] B. Lüthi, *Physical Acoustics in the Solid State* (Springer, Berlin, 2005).

[16] N. Bender, S. Factor, J. D. Bodyfelt, H. Ramezani, D. N. Christodoulides, F. M. Ellis, and T. Kottos, Observation of Asymmetric Transport in Structures with Active Nonlinearities, Phys. Rev. Lett. **110**, 234101 (2013).

[17] F. Nazari, N. Bender, H. Ramezani, M. K. Moravvej-Farshi, D. N. Christodoulides, and T. Kottos, Optical isolation via $\mathcal{PT}$-symmetric nonlinear Fano resonances, Opt. Express **22**, 9574 (2014).

[18] S. Lepri and G. Casati, Asymmetric Wave Propagation in Nonlinear Systems, Phys. Rev. Lett. **106**, 164101 (2011).

[19] B. Peng, S. K. Öždemir, F. Lei, F. Monifi, M. Gianfreda, G. L. Long, S. Fan, F. Nori, C. M. Bender, and L. Yang, Nonreciprocal light transmission in parity-time-symmetric whispering-gallery microcavities, Nat. Phys. **10**, 394 (2014).

[20] B. Liang, B. Yuan, and J.-C. Cheng, Acoustic Diode: Rectification of Acoustic Energy Flux in One-Dimensional Systems, Phys. Rev. Lett. **103**, 104301 (2009).

[21] B. Liang, X. S. Guo, J. Tu, D. Zhang, and J. C. Cheng, An acoustic rectifier, Nat. Mater. **9**, 989 (2010).

[22] N. Boechler, G. Theocharis, and C. Daraio, Bifurcation-based acoustic switching and rectification, Nat. Mat. **10**, 665 (2011).

[23] L. Wang and B. Li, Phononics gets hot, Phys. World **21**, 27 (2008).

[24] B. Li, L. Wang, and G. Casati, Thermal Diode: Rectification of Heat Flux, Phys. Rev. Lett. **93**, 184301 (2004).

[25] R. Fleury, D. L. Sounas, C. F. Sieck, M. R. Haberman, and A. Alú, Sound isolation and giant linear nonreciprocity in a compact acoustic circulator, Science **343**, 516 (2014).

[26] H. Li and T. Kottos, Linear thermal circulator based on Coriolis forces, Phys. Rev. E **91**, 020101(R) (2015).

[27] S. Suwunnarat, H. Li, R. Fleischmann, and T. Kottos, Low-temperature linear thermal rectifiers based on Coriolis forces, Phys. Rev. E **93**, 042115 (2016).

[28] N. Goldman and J. Dalibard, Periodically Driven Quantum Systems: Effective Hamiltonians and Engineered Gauge Fields, Phys. Rev. X **4**, 031027 (2014).

[29] A. Eckardt and E. Anisimovas, High-frequency approximation for periodically driven quantum systems from a Floquet-space perspective, New J. Phys. **17**, 093039 (2015).

[30] A. P. Itin and M. I. Katsnelson, Effective Hamiltonians for Rapidly Driven Many-Body Lattice Systems: Induced Exchange Interactions and Density-Dependent Hoppings, Phys. Rev. Lett. **115**, 075301 (2015).

[31] H. Li, T. Kottos, and B. Shapiro, Floquet-Network Theory of Nonreciprocal Transport, Phys. Rev. Appl. **9**, 044031 (2018).

[32] H. Li, B. Shapiro, and T. Kottos, Floquet scattering theory based on effective Hamiltonians of driven systems, Phys. Rev. B **98**, 121101(R) (2018).

[33] One can generalize the notion of "physical loops" to include configurations where modes are connected together to form a loop (closed path) in the mode space. In this case, the term "physical" refers to the fact that these loops are present even in the absence of driving.

[34] M. Rodriguez-Vega, M. Lentz, and B. Seradjeh, Floquet perturbation theory: Formalism and application to low-frequency limit, New J. Phys. **20**, 093022 (2018).

[35] A. Eckardt, Colloquium: Atomic quantum gases in periodically driven optical lattices, Rev. Mod. Phys. **89**, 011004 (2017).

[36] Y. V. Fyodorov and H.-J. Sommers, Statistics of resonance poles, phase shifts and time delays in quantum chaotic scattering: Random matrix approach for systems with broken time-reversal invariance, J. Math. Phys. **38**, 1918 (1998).

[37] H. Li, S. Suwunnarat, and T. Kottos, Statistical design of chaotic waveforms with enhanced targeting capabilities, Phys. Rev. B **98**, 041107(R) (2018).

[38] We remark that one-mode driving cannot lead to isolation with $O(1/\omega)$ performance, which is obvious when setting

$M = 2$ in Eq. (5) and considering that both the effective Hamiltonian $\hat{H}_F$ and the micromotion $\hat{u}_n$ are scalar in this case. Notice that we exclude the possibility of the lead-lead coupling, which is not captured by Eq. (5) [39].

between the effective Hamiltonian $\hat{H}_F$ and the micromotion within order $O\left(1/\omega^2\right)$, which, however, is beyond the current purpose to design $O\left(1/\omega\right)$ asymmetry in the nonreciprocal components.

[39] H. Li, B. K. Agarwalla, and J.-S. Wang, Generalized Caroli formula for the transmission coefficient with lead-lead coupling, Phys. Rev. E **86**, 011141 (2012).

[40] K. Fang, Z. Yu, and S. Fan, Realizing effective magnetic field for photons by controlling the phase of dynamic modulation, Nat. Photonics **6**, 782 (2012).

[41] For the example Eq. (9) (and similarly the previous one (14)), the effect of the micromotion is absent within order $O\left(1/\omega^2\right)$. It will be interesting to work with the complex Hermitian Hamiltonian $\hat{H}_0\left(t\right)$ to investigate the interplay

[42] N. A. Estep, D. L. Sounas, J. Soric, and A. Alu, Magnetic-free non-reciprocity and isolation based on parametrically modulated coupled-resonator loops, Nat. Phys. **10**, 923 (2014).

[43] M. Chitsazi, H. Li, F. M. Ellis, and T. Kottos, Experimental Realization of Floquet P T-Symmetric Systems, Phys. Rev. Lett. **119**, 093901 (2017).

[44] R. Fleury, D. L. Sounas, and A. Alú, Subwavelength ultrasonic circulator based on spatiotemporal modulation, Phys. Rev. B **91**, 174306 (2015).